



# Influence of Double Magnetic Fields on The Heat Transfer and Total Entropy Generation for Nanoliquid

Rached Miri<sup>1\*</sup>, Raoua Fattoum<sup>1</sup>, Bouchmel Mliki<sup>1</sup>, Mohamed Ammar Abassi<sup>1\*\*</sup>,  
Ammar Hidouri<sup>1</sup>

<sup>1</sup> Research Lab, Technology Energy and Innovative Materials, Faculty of Sciences, University of Gafsa, Tunisia

\*Rached Miri, Email address: [rachedmiri111@gmail.com](mailto:rachedmiri111@gmail.com)

\*\*Mohamed Ammar Abassi, Email address: [abbassima@gmail.com](mailto:abbassima@gmail.com)

Received 21 July 2024,  
Revised 28 Sept 2024,  
Accepted 01 Oct 2024

## Keywords:

- ✓ Magnetohydrodynamic,
- ✓ nano-liquid,
- ✓ Lattice Boltzmann approach,
- ✓ entropy generation

**Citation:** Miri R., Fattoum R., Mliki B., Abassi M. A., Hidouri A. (2024) Influence of Double Magnetic Fields on The Heat Transfer and Total Entropy Generation for Nanoliquid, *J. Mater. Environ. Sci.*, 15(10), 1347-1367

**Abstract:** This work studies laminar forced convection of nano-liquid in a rectangular channel with three cylindrical blocks. Two external magnetic fields are imposed. This phenomenon is simulated using the 2D Lattice Boltzmann approach. This paper investigates the effects of the following parameters: Reynolds number, Hartmann number, and nanoparticles volume fraction. The ranges of the main parameters are: ( $10 \leq Re \leq 100$ ), ( $0 \leq Ha_1 \leq 50$ ), ( $0 \leq Ha_2 \leq 50$ ), ( $0\% \leq \phi \leq 4\%$ ). The obtained results show that the average Nusselt number enhances according to the value of Reynolds number, and nanoparticles volume fraction. The impact of the horizontal magnetic force on the flow is more effective than that of the perpendicular magnetic force. And this is more remarkable when the conductive mode dominates. The value of total entropy generation  $S_{gen}$  increases by about 94.55%, when the Reynolds number is enhanced from 10 to 100. It increases by about 81.48% and 83.53% when the values of the horizontal magnetic field ( $Ha_1$ ) and the perpendicular magnetic field ( $Ha_2$ ) are increased from 0 to 50, respectively. Also, these parameters decrease with the addition of the nanoparticles ( $\phi=0.04$ ). to the base liquid by about 4.62%, for Reynolds number ( $Re=100$ ). The value of Bejan number reduces with Reynolds number, and with horizontal and vertical magnetic force. It is augmented by about 6.05%, and 12.03% when the nanoparticle volume fraction is equal to 0.04 for  $Re=25$ ; and 100, respectively.

## 1. Introduction

Forced convective heat transfer on a heated circular cylinder has many applications, such as the refrigeration cycle condensers, shell and tube type heat exchangers, probes or sensors in the measuring devices, pin fins, cooling towers, power electronics cooling, power generators, nuclear reactor, fuel element cooling, cylindrical cooling devices, and food processing.

Traditional coolants such as water or air are not optimal because of their relatively low thermal conductivity. Adding suitable nanoparticles to these fluids usually increases their thermal conductivity and is also effective for other fluid properties, such as thermophysical ones. Improving heat transfer efficiency is a desired goal. The addition of nanoparticles in a base fluid is one solution among several to improve the heat transfer rate.

Choi *et al.*, 1995, were the first to use this new type of fluid. The experimental results demonstrated that the addition of nanoparticles enhances the thermal conductivity of fluids. To verify these results several numerical and experimental research works have focused on the advantages of this new fluid (Ravisankar *et al.*, 2013), (Abbassi *et al.*, 2018), (Abbassi *et al.*, 2018), (Miri *et al.*, 2022), (Mliki *et al.*, 2017), (Esfe *et al.*, 2015), (Bazdidi-Tehrani *et al.*, 2019), (Esfe *et al.*, 2016), (Bahiraei *et al.*, 2018), (Bazdidi-Tehrani *et al.*, 2018), (Vasefi *et al.*, 2019), (Bahiraei *et al.*, 2017). The results show that the use of nanofluid enhances the heat transfer rate. Also, nanofluids in heat exchangers as studied by several works (Khairul *et al.*, 2014), (Barzegarian *et al.*, 2016), (Omiddezyani *et al.*, 2019), (Huang, Z *et al.*, 2015), the results have demonstrated that the using of nanofluids has a positive impact on heat transfer in heat exchangers.

Other works have focused on the use of Magnetohydrodynamic MHD forced convection of nanofluid, as a topic of interest for many researches. In this context, (Nikelham *et al.*, 2015) conducted research on the influence of magnetic field direction on the forced convection phenomenon of an aluminum oxide-water nanofluid flowing over a circular cylinder. The results reported that the rate of heat transfer is dependent directly on the Reynolds number, the volume fraction of the nanofluid, the Hartmann number, and the angle of the magnetic field. (Karimipour *et al.*, 2019) investigated numerically the laminar MHD forced convection flow of (water/FMWNT carbon nanotubes) in a microchannel imposed the uniform heat flux. The results have shown that the fully developed velocity profile varied with the Hartmann number, this means that increasing the magnetic field strength to increase the heat transfer rate is applicable only in a limited range, and it is not effective beyond that range. Forced convective heat transfer of nanofluids in porous half-rings has been studied in the presence of a uniform magnetic field by (Sheikholeslami *et al.*, 2017), (Miri *et al.*, 2024). The results indicated that the Nusselt number reduces with an increase in Lorentz forces. (Tumse *et al.*, 2022) studied the influence of the non-uniform magnetic field on the flow and thermal characteristics of a ferrofluid on a channel with a circular cylinder. The results show that the presence of a non-uniform magnetic field reduces the length of recirculation bubbles behind the cylinder block and changes the flow structure from an unsteady state to a steady state. This is due to the influence of Lorentz forces, which tend to dampen vortex diffusion. (Aminossadati *et al.*, 2011) studied the magnetic field impact on forced convection of Al<sub>2</sub>O<sub>3</sub>-water in a partially heated microchannel. The results reported that the microchannels are better in terms of heat transfer for higher Reynolds and Hartmann numbers. (Hamad *et al.*, 2011) studied the effect of magnetic field on free convection of three types of nanofluids: copper/water, alumina/water, and silver/water. The numerical results show that the increasing of the values of the magnetic parameter leads to a diminution of the velocity profiles and to enhance the thermal profiles for fixed values of nanoparticles concentrations. (Sheikholeslami *et al.*, 2016) studied the impact of an external magnetic field on forced convection of ferrofluid (Fe<sub>3</sub>O<sub>4</sub>-water). They found that the Nusselt number is a decreasing function of the Hartmann number. (Selimefendigil *et al.*, 2020) interspersed by the role of magnetic field on forced convection of CuO-water. The results found that the Hartmann number has positive effects on the average Nusselt number, and it is varied with the inclination angle of the lower branching channel. (Ishak *et al.*, 2009) studied the magnetohydrodynamic mixed convection flow. The results show that the magnetic field parameter plays a significant role in controlling the boundary layer separation. (Selimefendigil *et al.*, 2018) discussed the role of magnetohydrodynamics on the forced convection of CuO-water flow in a channel with four circular cylinder blocks. The results show that the average Nusselt number is enhanced by about 9.34% when the value of the Hartmann number is increased from Ha=5 to Ha=10. According to (Udhayakumar *et*

al., 2016) the influence of the magnetic field may contribute or hamper the convective heat transfer and the drag coefficient depending on its magnitude and direction. The main observation of the study by (Tassone et al., 2018) is that the average Nusselt number increases by about 20% when the magnetic field is applied.

Many studies involve magnetohydrodynamic forced convection flow in pipes. The present study becomes the first report on the influence of multi-magnetic fields on the heat transfer and the entropy generation of laminar forced convection flow of nano-liquid (copper/water) in a channel with three cylindrical blocks.

## Geometric configuration and mathematical formulation

### 2.1 Problem consideration

This present paper simulations were conducted in a 2D rectangular channel crossed by Cu–water nano-liquid and containing three-cylinder hot blocks. The channel has a length ( $L=21H$ ) and height ( $H$ ). The first hot cylinder block of diameter ( $D=H/2$ ) is placed in the middle of the channel in the  $Y$  direction and its center in the  $X$  direction is located at ( $L1=2.5H$ ). The distance between the cylinders is equal to ( $2.5H$ ). A uniform temperature is imposed on the three-cylinder blocks and the bottom wall. Two external magnetic flux with density  $B_0$  are applied, their orientation forms an angle ( $\gamma_1$  and  $\gamma_2$ ). This configuration is described in Figure 1. The thermophysical properties of the base liquid and the copper nanoparticles are presented in Table 1.

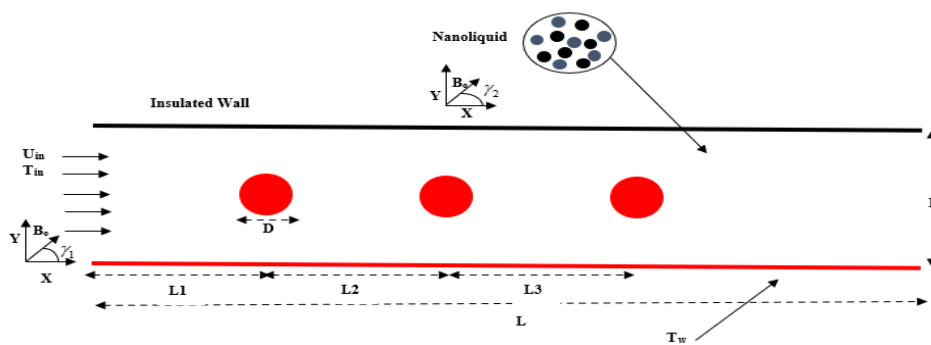


Figure 1. The schematic of the physique problem

Table 1. Thermo-physical properties of base water and the Cu nanoparticle

Physical properties	Water	Cu
$Cp(J.kg^{-1}.K^{-1})$	4181.8	383.1
$\rho(kg.m^{-3})$	1000.52	8954
$k(W.m^{-1}.K^{-1})$	0.597	386
$\beta(K^{-1})$	$21 \times 10^{-5}$	$51 \times 10^{-6}$
$\sigma(\Omega.m)^{-1}$	0.05	$2.7 \times 10^{-8}$
$\mu \times 10^4 (kg/m.s)$	8.55	-

## 2.2 Governing equations

The non-dimensionalizing Navier–Stokes and energy equations of MHD flow for the laminar forced convection in two-dimensional, for the single-phase can be written through the following equations (1-4) by substituting these dimensionless variables:

$$X = \frac{x}{H}, Y = \frac{y}{H}, U = \frac{u}{u_{in}}, \text{Pr} = \frac{\nu_{nl}}{\alpha_{nl}}, \theta = \frac{T - T_{in}}{T_w - T_{in}}, \text{Re} = \frac{u_{in} D_h}{\nu_{nl}}, P = \frac{p}{\rho u_{in}^2}, \text{Ha}_1 = HB_o \sqrt{\frac{\sigma_{nl}}{\mu_{nl}}}, \text{Ha}_2 = HB_o \sqrt{\frac{\sigma_{nl}}{\mu_{nl}}}$$

The governing equations in the dimensionless state can be written as follows:

$$\frac{\partial U}{\partial X} + \frac{\partial V}{\partial Y} = 0 \quad \text{Eqn. 1}$$

$$U \frac{\partial U}{\partial X} + V \frac{\partial U}{\partial Y} = -\frac{\partial P}{\partial X} + \frac{1}{\text{Re}} \left[ \frac{\partial^2 U}{\partial X^2} + \frac{\partial^2 U}{\partial Y^2} \right] + \quad \text{Eqn. 2}$$

$$\frac{\text{Ha}_1^2}{\text{Re}} (V \sin(\gamma_1) \cos(\gamma_1) - U \sin^2(\gamma_1)) + \frac{\text{Ha}_2^2}{\text{Re}} (V \sin(\gamma_2) \cos(\gamma_2) - U \sin^2(\gamma_2))$$

$$U \frac{\partial V}{\partial X} + V \frac{\partial V}{\partial Y} = -\frac{\partial P}{\partial Y} + \frac{1}{\text{Re}} \left[ \frac{\partial^2 V}{\partial X^2} + \frac{\partial^2 V}{\partial Y^2} \right] + \quad \text{Eqn. 3}$$

$$\frac{\text{Ha}_1^2}{\text{Re}} (U \sin(\gamma_1) \cos(\gamma_1) - V \cos^2(\gamma_1)) + \frac{\text{Ha}_2^2}{\text{Re}} (U \sin(\gamma_2) \cos(\gamma_2) - V \cos^2(\gamma_2))$$

$$U \frac{\partial \theta}{\partial X} + V \frac{\partial \theta}{\partial Y} = \frac{1}{\text{Pr} \cdot \text{Re}} \left( \frac{\partial^2 \theta}{\partial X^2} + \frac{\partial^2 \theta}{\partial Y^2} \right) \quad \text{Eqn. 4}$$

The boundary conditions of this problem are given in [Table 2](#):

**Table 2.** Boundary conditions

	Velocity boundary conditions	Temperature boundary conditions
At the inlet of channel	$U=1; V=0$	$\theta=0$
At the outlet of channel	$\frac{\partial U}{\partial X} = \frac{\partial V}{\partial X} = 0$	$\frac{\partial \theta}{\partial X} = 0$
At the downstream bottom wall of channel	$U=0; V=0$	$\theta=1$
At the top wall of channel	$U=0; V=0$	$\theta=0$
At the hot cylinder blocks	$U=0; V=0$	$\theta=1$

## 2.3 Nano-liquid properties

It is important to review the thermophysical parameters of nano-liquids and their mathematical models. The properties of nano-liquid are listed in [Table 3](#):



**Table 3.** Nano-liquid properties

Properties	Mathematical formulation
The heat capacitance	$(\rho C_P)_{nl} = (1 - \phi)(\rho C_P)_l + \phi(\rho C_P)_p$
Density	$\rho_{nl} = (1 - \phi)\rho_l + \phi\rho_p$
Thermal diffusivity	$\alpha_{nl} = k_{nl} / (\rho C_P)_{nl}$
Thermal conductivity	$k_{nl} = k_l \frac{k_p + 2k_l - 2\phi(k_l - k_p)}{k_p + 2k_l + \phi(k_l - k_p)}$
The viscosity thermal	$\mu_{nl} = \frac{\mu_l}{(1 - \phi)^{2.5}}$
The electrical conductivity	$\sigma_{nl} = \sigma_l \left[ 1 + \frac{3(\sigma_s / \sigma_l - 1)\phi}{(\sigma_s / \sigma_l + 2) - (\sigma_s / \sigma_l - 1)\phi} \right]$

### 2.4 Parameters of engineering interest

The main parameters of heat transfer, used to optimize or develop a forced convection heat transfer system, are examined in this study. The engineering parameters of interest can be calculated using the relations provided in **Table 4**:

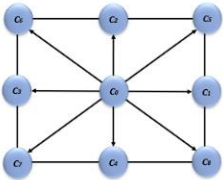
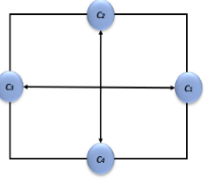
**Table 4.** The parameters of engineering interest

The local Nusselt number	$Nu = -\frac{k_{nl}}{k_l} \left( \frac{\partial \theta}{\partial Y} \right) \Big _{Y=0}$
The average Nusselt number	$Nu_{avg} = \frac{1}{L} \int_0^L Nu \cdot dX$
The relationships between the stream function and velocity components	$\frac{\partial^2 \psi}{\partial X^2} + \frac{\partial^2 \psi}{\partial Y^2} = \frac{\partial U}{\partial Y} - \frac{\partial V}{\partial X}$
The local dimensionless entropy generation	$S_{gen} = S_{gen,h} + S_{gen,v} + S_{gen,M}$
The entropy generation term relative to the heat transfer irreversibility	$S_{gen,h} = \frac{k_{nl}}{k_l} \left[ \left( \frac{\partial \theta}{\partial X} \right)^2 + \left( \frac{\partial \theta}{\partial Y} \right)^2 \right]$
The entropy generation term corresponds to nanoliquid friction irreversibility	$S_{gen,v} = \chi \frac{\mu_{nl}}{\mu_l} \left\{ 2 \left[ \left( \frac{\partial U}{\partial X} \right)^2 + \left( \frac{\partial V}{\partial Y} \right)^2 \right] + \left[ \left( \frac{\partial U}{\partial Y} \right) + \left( \frac{\partial V}{\partial X} \right) \right]^2 \right\}$
The entropy generation term associated with the magnetic field irreversibility	$S_{gen,M} = \chi \times \left\{ \left[ Ha_1^2 \times \left[ (1 - \phi) + \phi \frac{\rho_s}{\rho_l} \right] \times [U \sin(\gamma_1) - V \cos(\gamma_1)]^2 \right] + \left[ Ha_2^2 \times \left[ (1 - \phi) + \phi \frac{\rho_s}{\rho_l} \right] \times [U \sin(\gamma_2) - V \cos(\gamma_2)]^2 \right] \right\}$
The irreversibility factor	$\chi = \frac{\mu_l T_{in} U_{in}^2}{k_l (T_w - T_{in})^2}$
Bejan number	$Be_{Local} = \frac{S_{gen,h}}{S_{gen}}$

### 3. LBM method

The study applies the Lattice Boltzmann Method (LBM) to solve the Navier–Stokes and energy equations. To simulate flow and heat transfer of nano-liquid in a 2D canal. The following table outlines the discussion of this method.

**Table 5.** Dynamic field and temperature field with lattice Boltzmann approach

	Dynamic field	Temperature field
	D2Q9	D2Q4
Model		
Distribution function	$f_k(x + c_k \Delta t, t + \Delta t) = f_k(x, t) + \frac{\Delta t}{\tau_v} [f_k^{eq}(x, t) - f_k(x, t)] + \Delta t c_k F_k$	$g_k(x + c_k \Delta t, t + \Delta t) = g_k(x, t) + \frac{\Delta t}{\tau_g} [g_k^{eq}(x, t) - g_k(x, t)]$
Equilibrium distribution functions	$f_k^{eq} = \rho \omega_k \left[ \begin{array}{l} 1 + 3 \frac{c_k \cdot u_i}{c^2} + \\ \frac{9(c_k \cdot u_i)^2}{2c^4} - \frac{3u_i^2}{2c^2} \end{array} \right]$	$g_k^{eq} = \theta \omega_k [1 + 2c_k \cdot u_i]$

The macroscopic quantities are calculated by the following equations:

$$\rho = \sum_{k=0-8} f_k \quad \text{Eqn. 5}$$

$$\rho u = \sum_{k=0-8} f_k c_k + \Delta t F \quad \text{Eqn. 6}$$

$$\theta = \sum_{k=0-4} g_k \quad \text{Eqn. 7}$$

The unknown distribution functions are calculated by the following relations in **Table 6**:

**Table 6.** Boundary conditions for  $f$  and  $g$  distribution function

	Velocity boundary conditions	Temperature boundary conditions
	$\rho_{in} = \frac{f_0 + f_2 + f_4 + 2(f_3 + f_6 + f_7)}{1 - u_{inlet}}$	
At the inlet	$f_1 = f_3 + \frac{2}{3} \rho u_{inlet}$	$g_1 = \theta(\omega(1) + \omega(3)) - g_3$
	$f_5 = f_7 + \frac{1}{2}(f_4 - f_2) + \frac{1}{6} \rho u_{inlet}$	

$$f_8 = f_6 - \frac{1}{2}(f_4 - f_2) + \frac{1}{6}\rho u_{inlet}$$

---


$$f_3(n, j) = 2 \times f_3(n-1, j) - f_3(n-2, j)$$

At the outlet  
of the  
channel

$$f_6(n, j) = 2 \times f_6(n-1, j) - f_6(n-2, j) \quad g_3(n, j) = 2 \times g_3(n-1, j) - g_3(n-2, j)$$

$$f_7(n, j) = 2 \times f_7(n-1, j) - f_7(n-2, j)$$

---


$$f_4(i, m) = f_2(i, m)$$

At the top  
boundary

$$f_7(i, m) = f_5(i, m)$$

$$g_4(i, m) = g_4(i, m-1)$$

$$f_8(i, m) = f_6(i, m)$$

At the  
heated part  
of the walls

---


$$g_4(i, m) = \theta(\omega(4) + \omega(2)) - g_2(i, m)$$


---

## 4. Physical interpretations and discussion

### 4.1 Independence from iteration number

**Table 7** indicates the number of iterations required for results to be independent of the grid size. The iteration numbers selected for the study ranged from 1000 to 200000 for the nano-liquid in Reynolds number of 100. In this investigation, the independence of flow and heat transfer parameters is intended. For the chosen iteration number, the amounts of average Nusselt number on the bottom wall has been compared in different iterations number. According to the changes of parameters in the chosen iteration number, it is observed that the iteration number of 50,000, in comparison with less iterations number, has more accurate results. In this study, this iteration number has been used as an acceptable iteration number in the simulation of the numerical solving domain of heat transfer and flow.

**Table 7.** Average Nusselt number on the bottom wall for different iteration numbers

Iteration number	1000	5000	10000	50000	100000	200000
Average Nusselt number	52.870	26.228	16.127	13.338	13.339	13.339

### 4.2 Validation of the numerical code

To verify the accuracy of the current results, we compared the results for the local Nusselt number with those reported by (Atashafrooz *et al.*, 2019) and (Santar *et al.*, 2009). These comparisons show excellent agreement (**Figure. 2 and 3**).

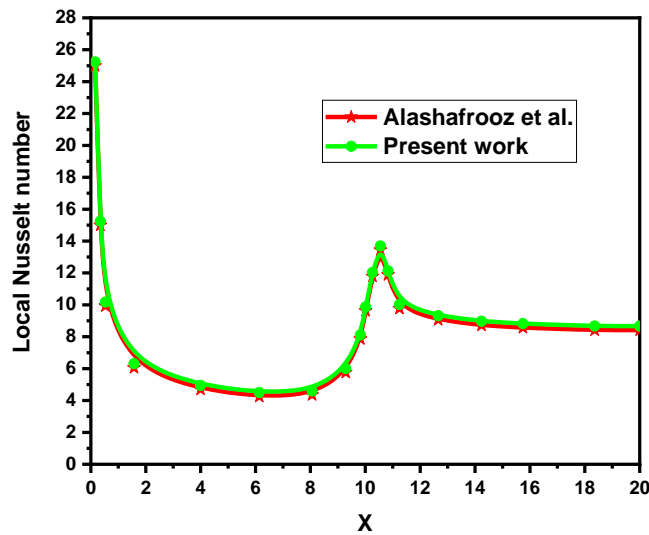


**Figure 2.** Local Nusselt number variation compared to those of (Alashafrooz *et al.*, 2019) for  $Re=400$ ;  $\phi=0.04$

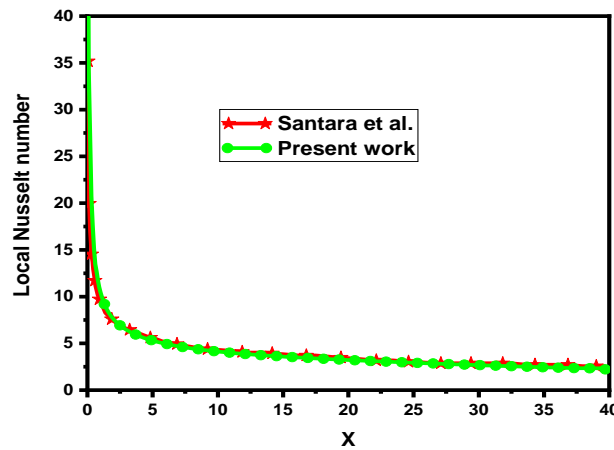


**Figure 3.** Comparison of the Nusselt number distribution along the bottom wall with results obtained by (Santar *et al.*, 2009) for  $Re=100$ ;  $\phi=0.025$

### 4.3 Independency from grid

The corresponding values of the average Nusselt number along the bottom wall are calculated and tabulated for several different grids in **Table 8**. According to this Table, the numerical results are almost the same for mesh smaller than  $840 \times 80$ , so there is no notable change in the results. Thus, an  $840 \times 80$  mesh was selected to implement the code. All computations in this research are performed using a computer program written in Fortran 90.

**Table 8.** Grid independence test results for  $Re=50$ ;  $\phi=0.02$ ;  $Ha_1=0$ ;  $\gamma_1=0^\circ$

Grid size	$Nu_{avg}$	Percentage of the difference
$105 \times 10$	6.123	—
$210 \times 20$	6.421	4.86%
$420 \times 40$	6.569	2.30%
$840 \times 80$	6.571	0.03%
$1680 \times 160$	6.572	0.015%

## 5. Results

### 5.1 Effects of Reynolds number

**Figure 4** illustrates the direct influence of inertia forces as represented by the Reynolds number, on the streamline and isotherm plots for  $Ha_1=0$ ;  $Ha_2=25$ ;  $\phi=0.02$ ;  $\gamma_1=0^\circ$ ;  $\gamma_2=-90^\circ$ ;  $\phi=0.02$ . The impact of this parameter is remarkable and clearly observed in this figure. The numerical results demonstrate that streamline multiplies when the value of the Reynolds number increases from 10 to 100. The maximum value of  $(\psi_{max})$  increases by nearly 16.02% when the Reynolds number reaches 100. Moreover, recirculation zones are generated as this parameter improves. This is due to the presence of cylindrical obstacles; which allow alter the flow direction of the streamline. On the other side, the isotherm lines are more compressed, this means that the convection mode dominates dependently on the inertia forces.

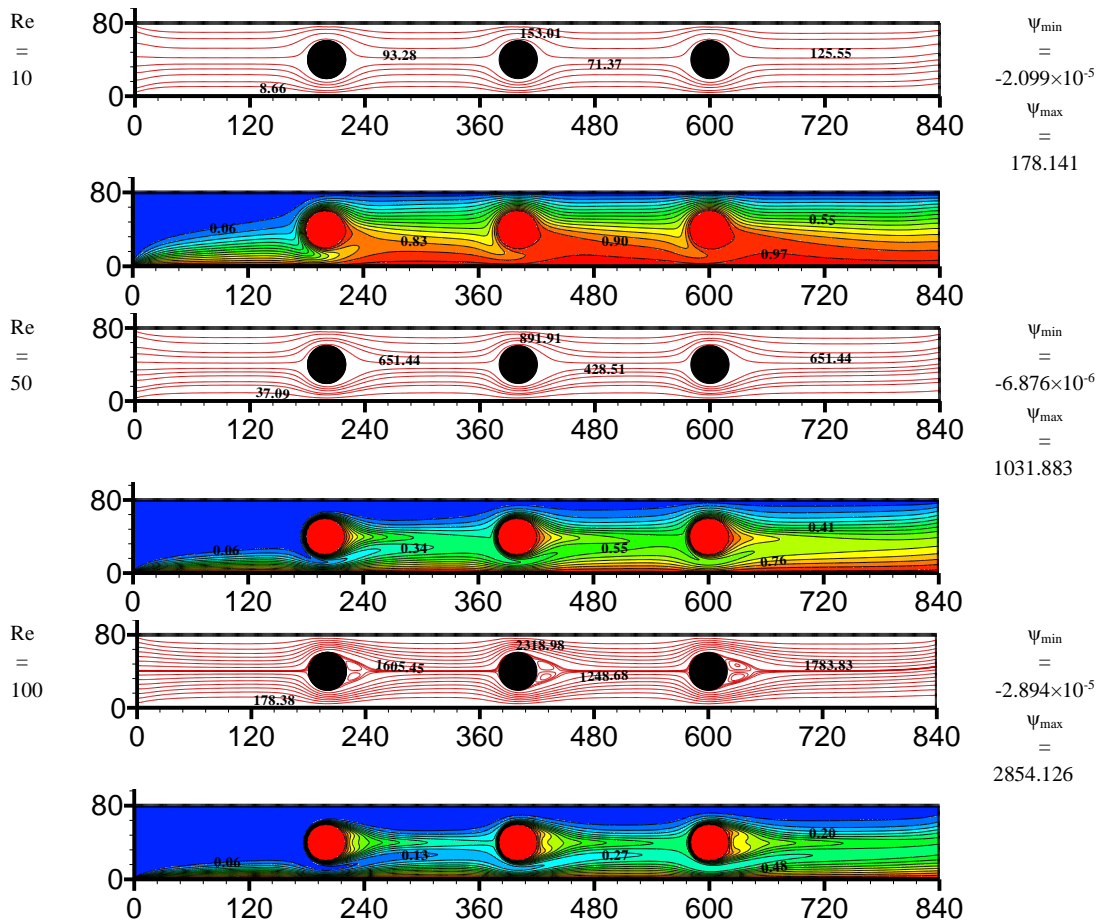


**Figure 4.** Impact of Reynolds number on streamline and isotherm contour for  $Ha_1=0$ ;  
 $Ha_2=25$ ;  $\phi=0.02$ ;  $\gamma_1=0^\circ$ ;  $\gamma_2=-90^\circ$

The enhancement of heat transfer rates, as expressed by the average Nusselt number, is depicted in **Figure 5**. The influence of Reynolds number on  $Nu_{avg}$  for  $0 \leq Ha_1 \leq 50$ ;  $0 \leq Ha_2 \leq 50$ ;  $\phi=0.02$ ;  $\gamma_1=0^\circ$ ;  $\gamma_2=-90^\circ$ , is studied numerically. The curve of the Nusselt number as a function of this non-dimensional number (Re). The simulation results show that the increase in inertia forces strengthens the heat transfer rate of nano-liquid. For example, at  $Ha_1=50$ ;  $Ha_2=0$ ;  $\phi=0.02$ ;  $\gamma_1=0^\circ$ ;  $\gamma_2=-90^\circ$ , the average Nusselt number multiplies about 3.8 when the number of Reynolds increases from 10 to 100. These results are confirmed by other studies such as Ref. (Miri et al., 2023), (Alsabery et al., 2021).

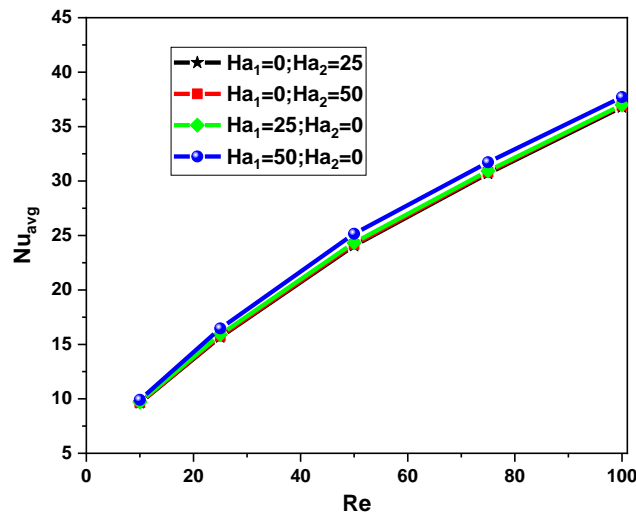


**Figure 5.** Impact of Reynolds number on  $Nu_{avg}$  for  $0 \leq Ha_1 \leq 50; 0 \leq Ha_2 \leq 50$ ;  $\phi=0.02; \gamma_1=0^\circ; \gamma_2=-90^\circ$

The impact of Reynolds number on the  $S_{gen}$  for  $0 \leq Ha_1 \leq 50; 0 \leq Ha_2 \leq 50$ ;  $\phi=0.02; \gamma_1=0^\circ; \gamma_2=-90^\circ$ , are shown in **Figure 6**. The curve of the total entropy generation depends directly by the value of the Reynolds number. The value of  $S_{gen}$  increases and is more remarkable for a higher Reynolds number ( $Re=100$ ). Approximately 94.55% increase in total entropy generation can be achieved when  $Ha_1=0; Ha_2=50$ . It is due to the entropy generation parameter corresponding to nano-liquid friction irreversibility. Consequently, the irreversibility of nano-liquid improves dependently on the inertia forces.

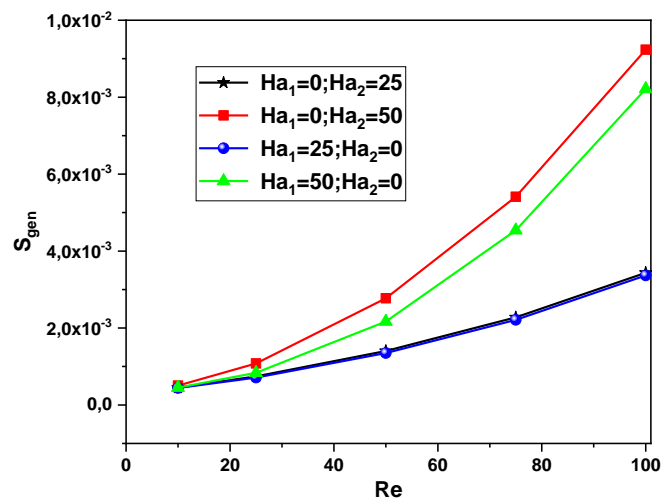


**Figure 6.** Impact of Reynolds number on  $S_{gen}$  for  $0 \leq Ha_1 \leq 50; 0 \leq Ha_2 \leq 50$ ;  $\phi=0.02; \gamma_1=0^\circ; \gamma_2=-90^\circ$

**Figure 7** explains the influence of Reynolds number on  $Be$  for  $0 \leq Ha_1 \leq 50; 0 \leq Ha_2 \leq 50$ ;  $\phi=0.02; \gamma_1=0^\circ; \gamma_2=-90^\circ$ . The impact of this parameter on the entropy generation observed in this curve. Bejan number which represents the ratio of entropy generation rates due to heat transfer and nano-liquid friction shows reduction. A higher value of the Reynolds number results in lower values of the Bejan number. The values of Bejan numbers are below 0.2 for  $Re=100$  which indicates that the entropy generation of the nano-liquid friction irreversibility is dominant over the heat transfer irreversibility.



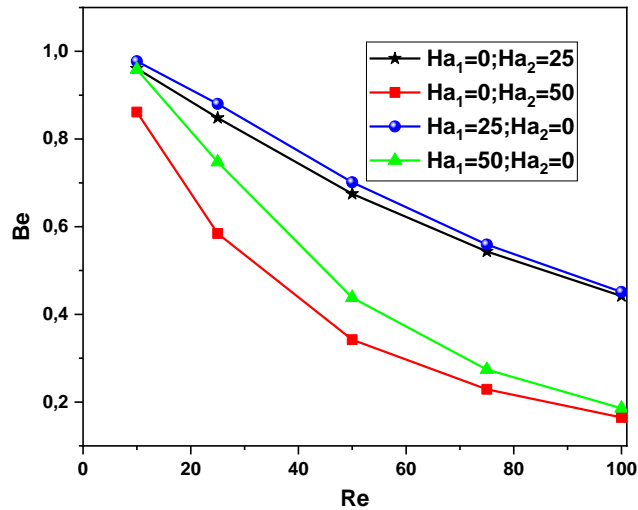


**Figure 7.** Impact of Reynolds number on Be for  $0 \leq Ha_1 \leq 50; 0 \leq Ha_2 \leq 50;$   
 $\phi=0.02; \gamma_1=0^\circ; \gamma_2=-90^\circ$

### 5.2 Influence of magnetic field

In this section, numerical simulation focuses on the influence of external volumetric force. **Figure 8** describes the impact of the horizontal magnetic field in terms of  $Ha_1$  on the streamline and isotherm contour for  $Re=100; Ha_2=50; \phi=0.02; \gamma_1=0^\circ; \gamma_2=-90^\circ$ . The external volumetric force is parallel to the flow of the nano-liquid. Recirculation zones generated due to the increase in inertial force behind cylindrical obstacles are dispersed, and their volume decreases. It is due to the application of the Lorentz force; this volumetric force strengthens the current lines and enriches this term. Due to the enrichment of the current lines, these zones are eliminated. The maximum value of streamline multiply about 1.053 when the  $Ha_1=50$ , it is equal to 3044.248. We have observed that the minimum value of streamline tends towards 0, indicating a diminution in the recirculation zones. The isotherm lines are slightly compressed, resulting in a slight increase in the conductive mode.

**Figure 9** demonstrates the influence of the vertical magnetic field in term of  $Ha_2$  on the streamline and isotherm contour for  $Re=100; Ha_1=50; \phi=0.02; \gamma_1=0^\circ; \gamma_2=-90^\circ$ . The maximum value of streamline multiply about 1.017 when the  $Ha_2=50$ , it is equal to 3044.248. These results show that the impact of the magnetic force parallel to the flow is more effective than the case where the magnetic force is perpendicular to the nano-liquid flow. As we can see, a deformation of the recirculation zones has been detected. This deformation is observed in the upper part of these zones and is due to the position of the applied magnetic force. The minimum value of streamline tends towards 0, indicating a deformation of the recirculation zones.

**Figure 10** represents the impact of the horizontal magnetic field ( $Ha_1$ ) on  $Nu_{avg}$  for  $25 \leq Re \leq 100; Ha_2=0; \phi=0.02; \gamma_1=0^\circ; \gamma_2=-90^\circ$ . As can be seen by increasing the value of  $Ha_1$ , it gives enhancement of heat transfer in term of  $Nu_{avg}$ . The value of the average Nusselt number increases by about 4.96 % for  $Re=25$ , and it is developed by about 2.56% for  $Re=100$  which demonstrates that the application of horizontal magnetic field has a positive impact on  $Nu_{avg}$ . The reason for this behavior is that the flow is steady at higher Hartmann number  $Ha_1$  values. It can be noted that this influence is more remarkable at a low value of Reynolds number. The physical reason for this phenomenon is the application of

horizontal Lorentz force. This external force reinforced the heat transfer rate higher when the conductive mode dominates.

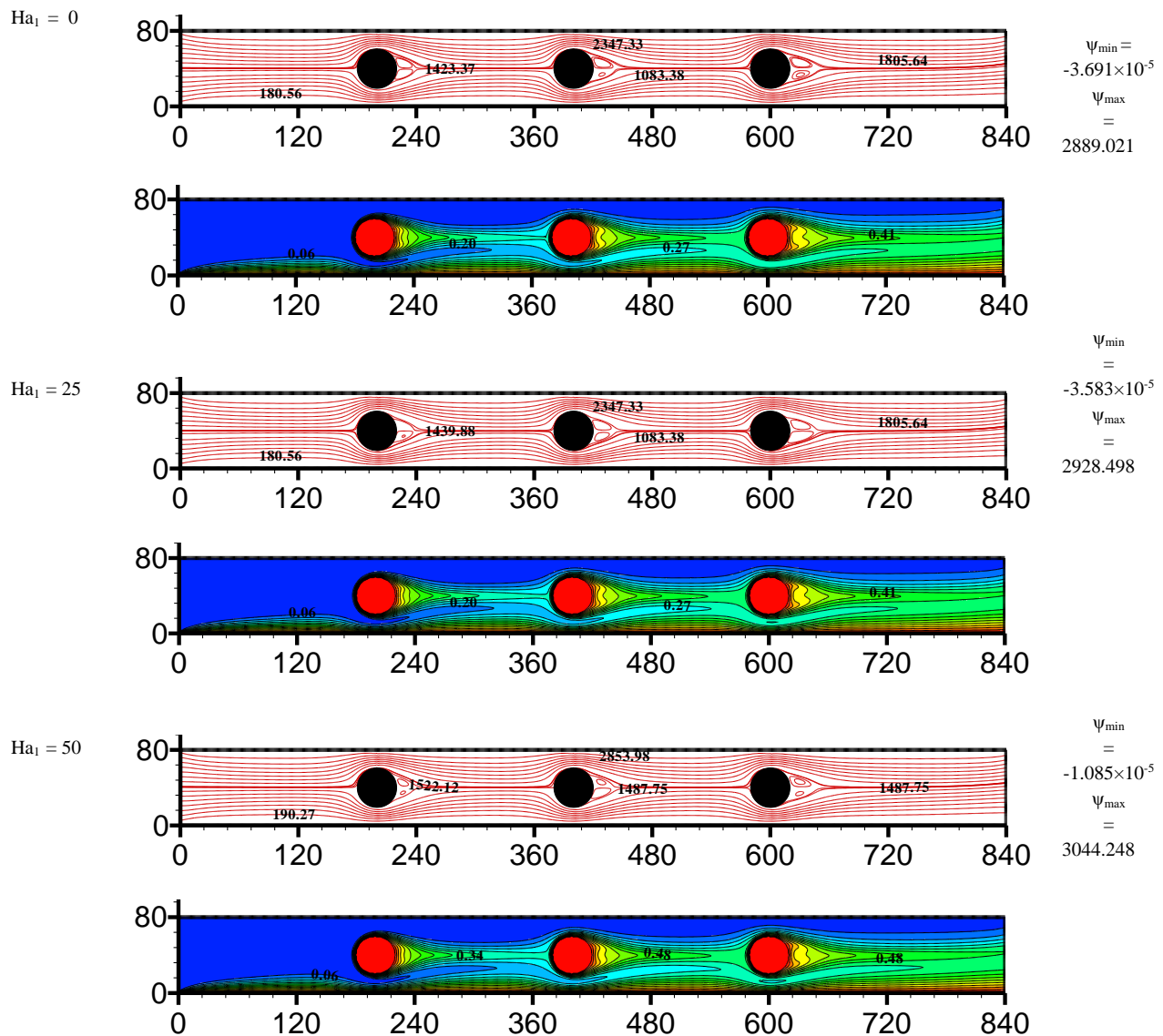


**Figure 8.** Impact of Hartmann number ( $Ha_1$ ) on streamline and isotherm contour for  $Re=100$ ;  $Ha_2=50$   
 $\phi=0.02$ ;  $\gamma_1=0^\circ$ ;  $\gamma_2=-90^\circ$

**Figure 11** illustrates the variation of the average Nusselt number in function of ( $Ha_2$ ) for  $25 \leq Re \leq 100$ ;  $Ha_1=0$ ;  $\phi=0.02$ ;  $\gamma_1=0^\circ$ ;  $\gamma_2=-90^\circ$ . The vertical magnetic field ( $Ha_2$ ) enhances the heat transfer in term of  $Nu_{avg}$ . The average Nusselt number increases by about 0.65% for  $Re=25$ , and it is raised by about 0.50% for  $Re=100$  which indicates that the vertical magnetic field has a slight positive impact on  $Nu_{avg}$ . Also, at a low value of Reynolds number, the effect of the vertical magnetic field is more remarkable. The physical reason for this phenomenon is the presence of Lorentz force. The perpendicularity of this volumetric force on the flow of nano-liquid is the main responsible for the slight increase on heat transfer rates.

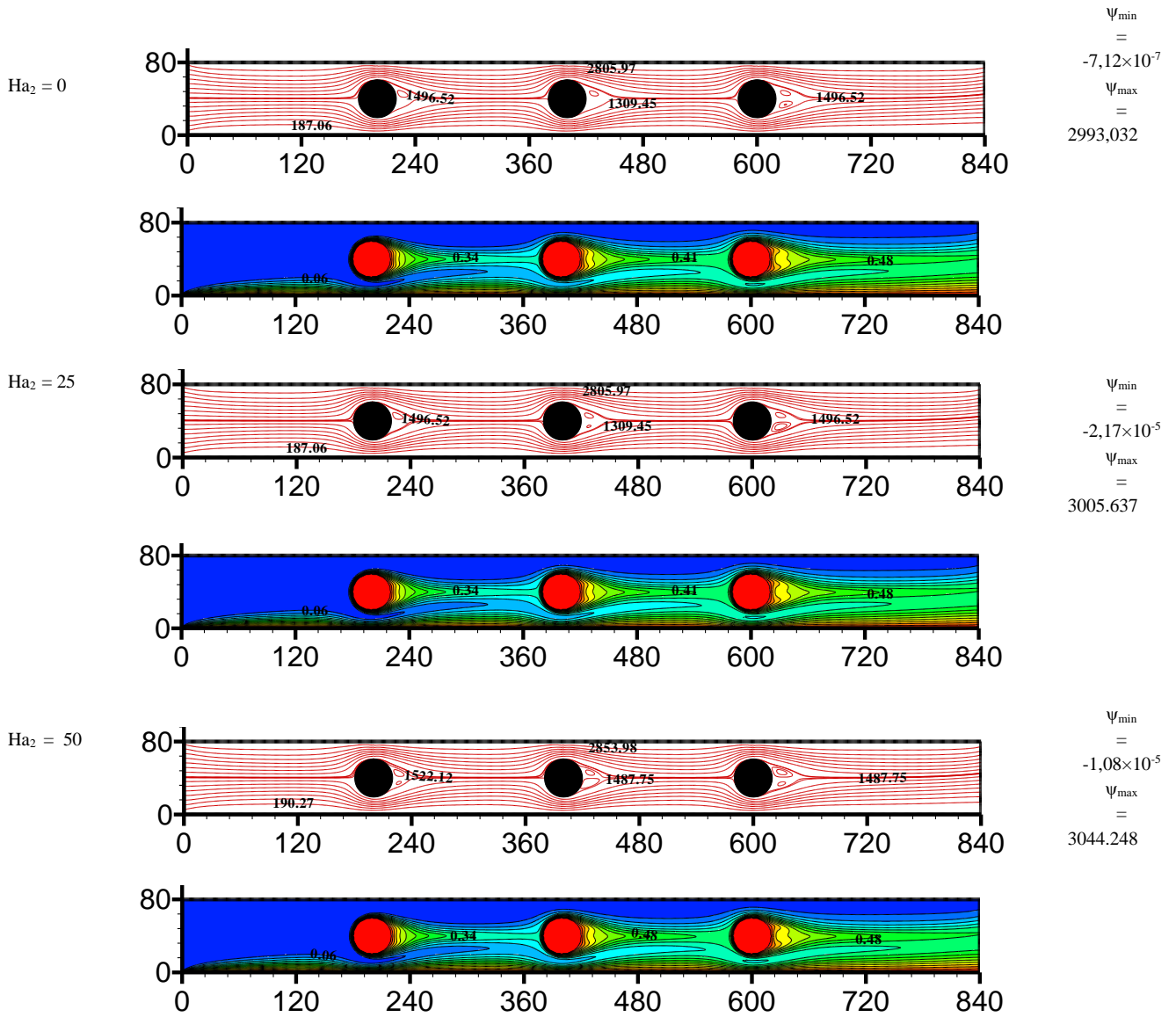


**Figure 9.** Impact of Hartmann number ( $Ha_2$ ) on streamline and isotherm contour for  $Re=100$ ;  $Ha_1=50$   $\phi=0.02$ ;  $\gamma_1=0^\circ$ ;  $\gamma_2=-90^\circ$

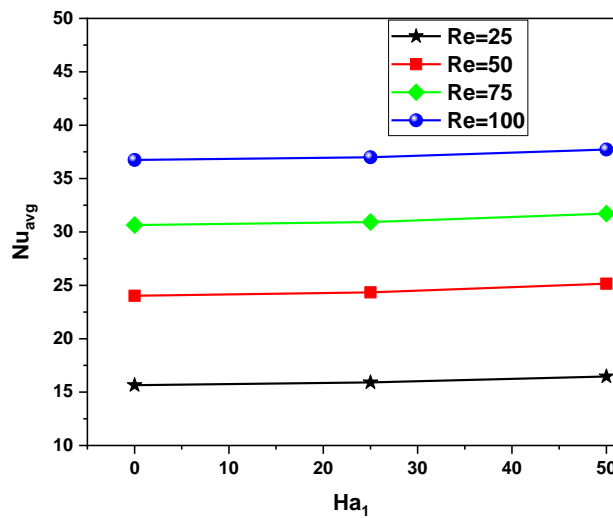


**Figure 10.** Impact of Hartmann number  $Ha_1$  on  $Nu_{avg}$  for  $25 \leq Re \leq 100$ ;  $Ha_2=0$ ;  $\phi=0.02$ ;  $\gamma_1=0^\circ$ ;  $\gamma_2=-90^\circ$

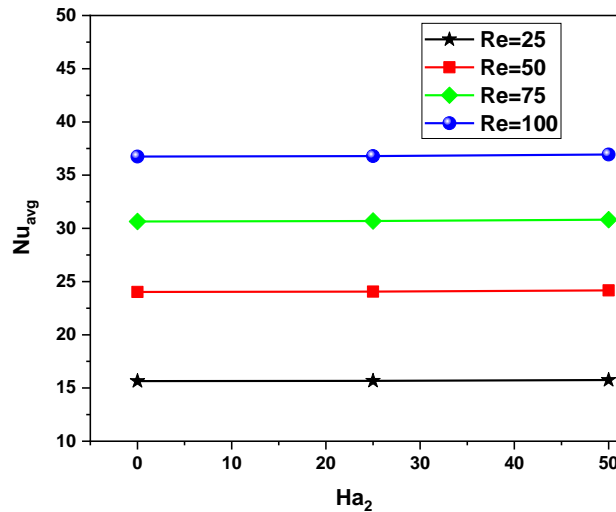


**Figure 11.** Impact of Hartmann number  $Ha_2$  on  $Nu_{avg}$  for  $25 \leq Re \leq 100$ ;  $Ha_1=0$ ;  $\phi=0.02$ ;  $\gamma_1=0^\circ$ ;  $\gamma_2=-90^\circ$

**Figure 12** shows the effect of the horizontal magnetic field ( $Ha_1$ ) on  $S_{gen}$  for  $25 \leq Re \leq 100$ ;  $Ha_2=0$ ;  $\phi=0.02$ ;  $\gamma_1=0^\circ$ ;  $\gamma_2=-90^\circ$ . The total entropy generation increases according to the value of Hartmann number ( $Ha_1$ ). This is signified that the disorder of the nano-liquid is enhanced when the value of the horizontal magnetic field augmented. The value of  $S_{gen}$  developed about 24.89% for  $Re=25$ , and 81.48% for  $Re=100$ . It is due to the enhancement of the entropy generation term relative to the heat transfer irreversibility and the entropy generation term associated with the horizontal magnetic field irreversibility.

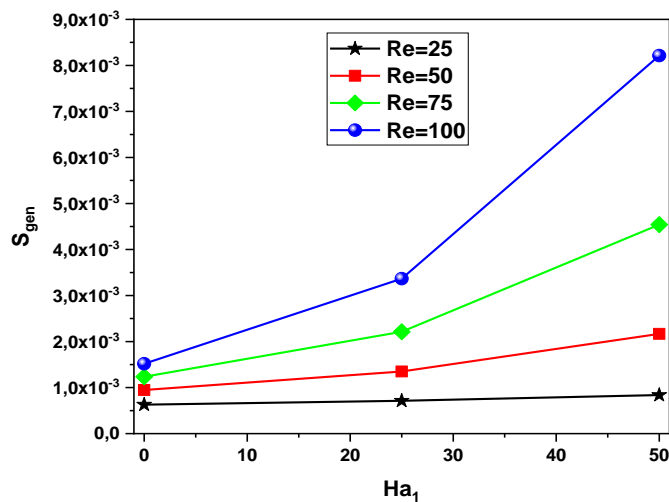


**Figure 12.** Impact of Hartmann number  $Ha_1$  on  $S_{gen}$  for  $25 \leq Re \leq 100$ ;  $Ha_2=0$ ;  $\phi=0.02$ ;  $\gamma_1=0^\circ$ ;  $\gamma_2=-90^\circ$

**Figure 13** shows the effect of the vertical magnetic field on  $S_{gen}$  for  $25 \leq Re \leq 100$ ;  $Ha_1=0$ ;  $\phi=0.02$ ;  $\gamma_1=0^\circ$ ;  $\gamma_2=-90^\circ$ . The value of total entropy generation increases according to the vertical magnetic field in term of the Hartmann number ( $Ha_2$ ). This is signified that the disorder of the nano-liquid is enhanced when the value of the vertical magnetic field augmented. The value of total entropy generation  $S_{gen}$

increased by about 41.85%; 83.53% for  $Re=25;100$ , respectively. It can be noted that the degree of disorder is higher depending on the vertical magnetic field, especially at higher value of Reynolds number. It is due to the enhancement of two terms the entropy generation term relative to the heat transfer irreversibility and then associated with the horizontal magnetic field irreversibility.

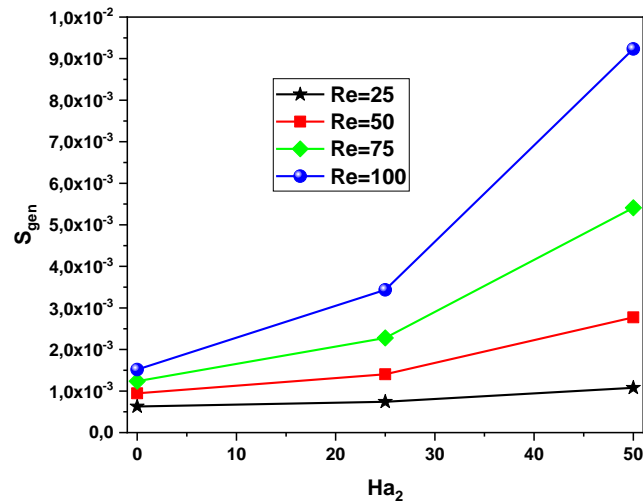


**Figure 13.** Impact of Hartmann number  $Ha_2$  on  $S_{gen}$  for  $25 \leq Re \leq 100$ ;  $Ha_1=0$ ;  $\phi=0.02$ ;  $\gamma_1=0^\circ$ ;  $\gamma_2=-90^\circ$

Figures 14 and 15 depict the effect of the horizontal and vertical magnetic field ( $Ha_1$  and  $Ha_2$ ) on Bejan number for  $25 \leq Re \leq 100$ ;  $Ha_2=0$ ;  $\phi=0.02$ ;  $\gamma_1=0^\circ$ ;  $\gamma_2=-90^\circ$ . The value of the Bejan number reduces with the rise of the Hartmann number ( $Ha_1$  or  $Ha_2$ ). This indicates that the application of horizontal or vertical magnetic fields has a negative impact on the Bejan number. It is diminution about 438.29% when the horizontal magnetic field is appalled for  $Re=100$ ;  $Ha_2=0$ ;  $\phi=0.02$ ;  $\gamma_1=0^\circ$ ;  $\gamma_2=-90^\circ$ , and decreases this parameter for the same condition about 506,51% when the vertical magnetic field is appalled. Remarkably, the influence of the vertical magnetic field is higher than the horizontal magnetic field. This is due to the perpendicularity between the Lorentz force and the inertial force.

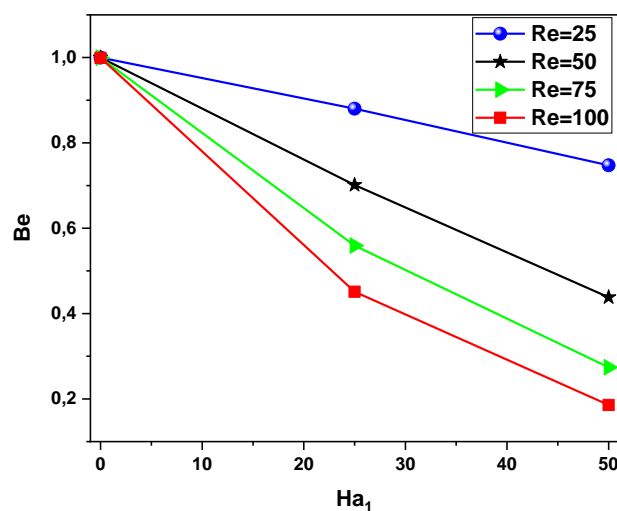


**Figure 14.** Impact of Hartmann number  $Ha_1$  on  $Be$  for  $25 \leq Re \leq 100$ ;  $Ha_2=0$ ;  $\phi=0.02$ ;  $\gamma_1=0^\circ$ ;  $\gamma_2=-90^\circ$

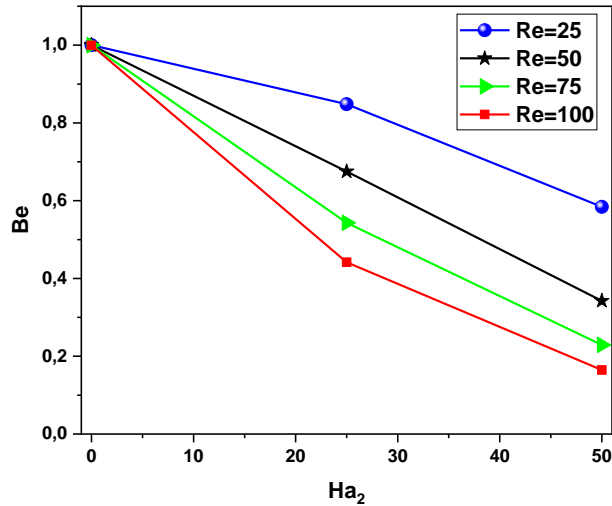


**Figure 15.** Impact of Hartmann number  $Ha_2$  on  $Be$  for  $25 \leq Re \leq 100$ ;  $Ha_1=0$ ;  $\phi=0.02$ ;  $\gamma_1=0^\circ$ ;  $\gamma_2=-90^\circ$

### 5.3 Effects of nanoparticles volume fraction

The Cu-water nano-liquid at different volumetric concentrations (0.01, 0.02, 0.03, and 0.04) is examined in the present simulation work.

The curve of the average Nusselt number ( $Nu_{avg}$ ) in the function of nanoparticles volume fraction for  $25 \leq Re \leq 100$ ;  $Ha_1=Ha_2=50$ ;  $\gamma_1=0^\circ$ ;  $\gamma_2=-90^\circ$  is shown in **Figure 16**. The average Nusselt number enhances progressively with increasing the value of nanoparticle volume fraction. This indicates that the heat transfer rate in term of ( $Nu_{avg}$ ) for nano-liquid is higher than the classic liquid. The addition of small nanoparticles ( $\phi=0.04$ ) to pure liquid improved the heat transfer performance by about 8.61% and 9.67% for  $Re=25$  and  $100$ ;  $Ha_1=Ha_2=50$ ;  $\gamma_1=0^\circ$ ;  $\gamma_2=-90^\circ$ . This positive impact is due to the higher thermal conductivity of nanoparticles.

The variation in the degree of disorder is expressed through the thermal of total entropy generation, and it depends on the nanoparticles' volume fraction. In **Figure 17**, we noticed a slight increase in total entropy generation  $S_{gen}$  when the conductive mode dominates ( $Re=25$ ) the addition of 0.04 of nanoparticle augmented the value of  $S_{gen}$  by about 2.8% for  $Re=25$ . The main responsible of this augmentation is the development of the entropy generation term relative to the heat transfer irreversibility. So, it can be concluded that the higher conductivity of nanoparticles enhances the entropy generation term relative to the heat transfer irreversibility ( $S_{gen,h}$ ) consequently the value of total entropy generation slightly increases.

On the other side, for a higher value of Reynolds number ( $Re=50;75;100$ ), the total entropy generation slightly decreases with the addition of the nanoparticles ( $\phi=0.04$ ) in base liquid about 1.77%; 3.74%; 4.62%, respectively. This is due to the domination of the convection mode, thus it can be concluded that the higher viscosity thermal of nanoparticles diminution the entropy generation term corresponds to nano-liquid friction irreversibility ( $S_{gen,v}$ ) consequently the value of total entropy generation slightly decreases.



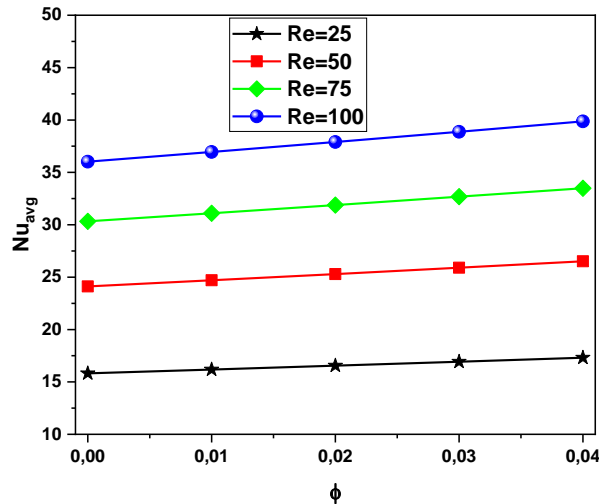


**Figure 16.** Impact of Nanoparticle concentrations ( $\phi$ ) on  $Nu_{avg}$  for  $25 \leq Re \leq 100$ ;  $Ha_1=Ha_2=50$ ;  $\gamma_1=0^\circ$ ;  $\gamma_2=-90^\circ$

The variation in the degree of disorder is expressed through the thermal of total entropy generation, and it depends on the nanoparticles volume fraction. In **Figure 17**, we noticed a slight increase in total entropy generation  $S_{gen}$  when the conductive mode dominates ( $Re=25$ ) the addition of 0.04 of nanoparticle augmented the value of  $S_{gen}$  about 2.8% for  $Re=25$ . The mains responsible of this augmentation is the developing of the entropy generation term relative to the heat transfer irreversibility. So it can be concluded that the higher conductivity of nanoparticles enhance the entropy generation term relative to the heat transfer irreversibility ( $S_{gen,h}$ ) consequently the value of total entropy generation slightly increase. In the author side, for higher value of Reynolds number ( $Re=50;75;100$ ), the total entropy generation slight decrease with the addition of the nanoparticles ( $\phi=0.04$ ) in base liquid about 1.77%; 3.74%; 4.62%, respectively. This is due to domination of the convection mode. So it can be concluded that the higher viscosity thermal of nanoparticles diminution the entropy generation term corresponds to nano\_liquid friction irreversibility ( $S_{gen,v}$ ) consequently the value of total entropy generation slightly decrease.

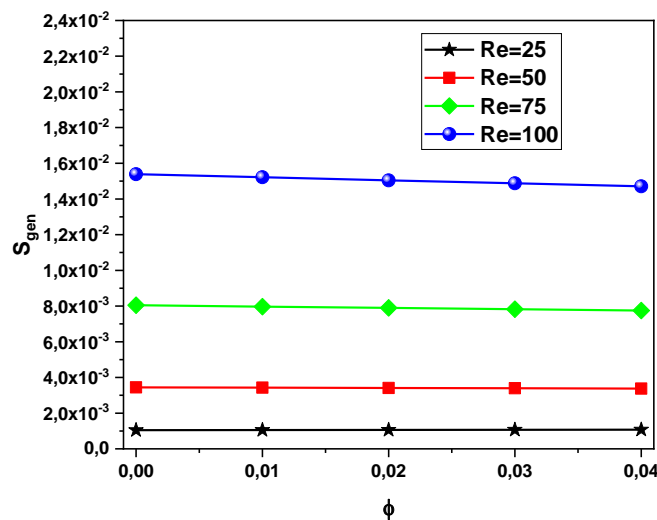


**Figure 17.** Impact of Nanoparticle concentrations ( $\phi$ ) on  $S_{gen}$  for  $25 \leq Re \leq 100$ ;  $Ha_1=Ha_2=50$ ;  $\gamma_1=0^\circ$ ;  $\gamma_2=-90^\circ$

**Figure 18** shows the impact of the nanoparticle concentrations ( $\phi$ ) on Be for  $25 \leq Re \leq 100$ ;  $Ha_1=Ha_2=50$ ;  $\gamma_1=0^\circ$ ;  $\gamma_2=-90^\circ$ . The value of Bejan numbers is affected by nanoparticle concentrations. This parameter enhances about 6.05%; 12.03% when nanoparticle volume fraction is equal to 0.04 for  $Re=25;100$ , respectively. This is due to the augmentation of the total entropy generation.

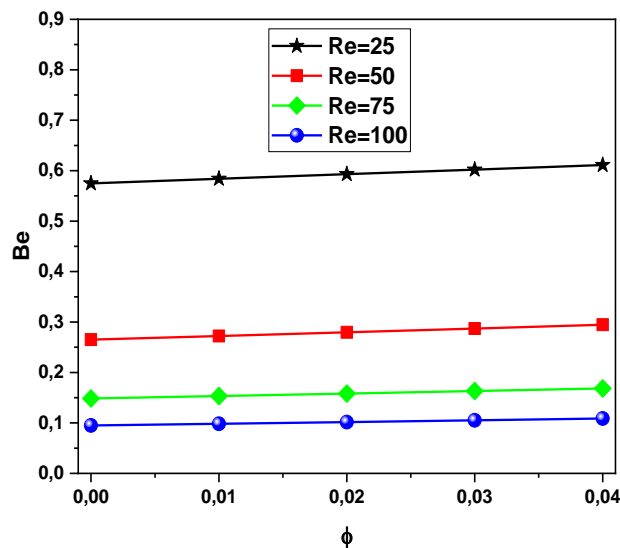


**Figure 18.** Impact of nanoparticle concentrations ( $\phi$ ) on Be for  $25 \leq Re \leq 100$ ;  $Ha_1=Ha_2=50$ ;  $\gamma_1=0^\circ$ ;  $\gamma_2=-90^\circ$

## Conclusion

This research investigates the laminar MHD forced convection flow of nano-liquid in a channel with three cylindrical blocks, in the presence of two magnetic fields. The LBM approach was used for the simulation of nano-liquid flow and heat transfer.

The focus has been on the influence of the Reynolds number ( $Re$ ), horizontal and vertical magnetic field ( $Ha_1$ ;  $Ha_2$ ), and nanoparticles volume fraction on streamlines and isotherms contours, average Nusselt number, total entropy generation ( $S_{gen}$ ) and Bejan number ( $Be$ ). The main findings of this work can be summarized as follows:

The average Nusselt number was multiplied about 3.8 when the number of Reynolds increases from 10 to 100.

The value of total entropy generation  $S_{gen}$  increases and is more remarkable for higher Reynolds number ( $Re=100$ ). Approximately 94.55% increase in  $S_{gen}$  can be achieved when  $Ha_1=0$ ;  $Ha_2=50$ .

The values of Bejan numbers are below 0.2 for the higher value of Reynolds number ( $Re=100$ ) which indicates that the entropy generation of the nano-liquid friction irreversibility is dominant over the heat transfer irreversibility.

The value of the average Nusselt number enhances about 4.96 % for  $Re=25$ , and it is developed about 2.56% for  $Re=100$  which demonstrates that the application of horizontal magnetic field has a positive impact on  $Nu_{avg}$ . This external force is more reinforced by the heat transfer rate when the conductive mode dominates.

The total entropy generation increases according to the value of the horizontal magnetic field ( $Ha_1$ ). It is developed about 24.89% for  $Re=25$ , and 81.48% for  $Re =100$ .

The average Nusselt number increases by about 0.65% for  $Re=25$ , and it is raised by about 0.50% for  $Re=100$  which indicates that the vertical magnetic field has a slight positive impact on  $Nu_{avg}$ .

The value of total entropy generation increases according to the vertical magnetic field in term of the Hartmann number ( $Ha_2$ ). It increases by about 41.85%; 83.53% for  $Re=25;100$ , respectively.

The application of a horizontal or a vertical magnetic field has a negative impact on the Bejan number. This influence is more remarkable with the vertical magnetic field.

The addition of ( $\phi=0.04$ ) nanoparticles to pure liquid improved the heat transfer performance in term of ( $Nu_{avg}$ ) about 8.61% and 9.67% for  $Re=25$  and 100.

The total entropy generation is enhanced by about 2.8% for  $Re=25$ , and it has a slight decrease with the addition of the nanoparticles ( $\phi=0.04$ ) in base liquid about 1.77%; 3.74%; 4.62%, for Reynolds number ( $Re=50;75;100$ ), respectively.

The value of Bejan numbers is affected by nanoparticle concentrations. This parameter enhances about 6.05%; 12.03% when nanoparticle volume fraction is equal to 0.04 for  $Re=25;100$ , respectively.

**Acknowledgement**, This work is carried out in Research Lab, Technology Energy and Innovative Materials, Faculty of Sciences, University of Gafsa, Tunisia.

## References

- Abbassi, M. A., Safaei, M. R., Djebali, R., Guedri, K., Zeghmami, B., Alrashed, A. A. (2018). LBM simulation of free convection in a nanofluid filled incinerator containing a hot block. *International Journal of Mechanical Sciences*, 144, 172-185. <https://doi.org/10.1016/j.ijmecsci.2018.05.031>
- Abbassi, M. A., Djebali, R., Guedri, K. (2018). Effects of heater dimensions on nanofluid natural convection in a heated incinerator shaped cavity containing a heated block. *Journal of Thermal Engineering*, 4(3), 2018-2036. doi: 10.18186/journal-of-thermal-engineering.411434
- Alsabery, A. I., Hajjar, A., Sheremet, M. A., et al. (2021). Impact of particles tracking model of nanofluid on forced convection heat transfer within a wavy horizontal channel. *International Communications in Heat and Mass Transfer*, 122, 105176, <https://doi.org/10.1016/j.icheatmasstransfer.2021.105176>
- Aminossadati, S. M., Raisi, A., Ghasemi, B. (2011). Effects of magnetic field on nanofluid forced convection in a partially heated microchannel. *International Journal of Non-Linear Mechanics*, 46(10), 1373-1382. <https://doi.org/10.1016/j.ijnonlinmec.2011.07.013>
- Atashafrooz, M., Sheikholeslami, M., Sajjadi, H., Delouei, A. A. (2019). Interaction effects of an inclined magnetic field and nanofluid on forced convection heat transfer and flow irreversibility in a duct with an abrupt contraction. *Journal of Magnetism and Magnetic Materials*, 478, 216-226. <https://doi.org/10.1016/j.jmmm.2019.01.111>
- Bahiraeei, M., Heshmatian, S. (2017). Efficacy of a novel liquid block working with a nanofluid containing graphene nanoplatelets decorated with silver nanoparticles compared with conventional CPU coolers. *Applied Thermal Engineering*, 127, 1233-1245. doi:10.1016/j.applthermaleng.2017.08.136
- Bahiraeei, M., Heshmatian, S., Keshavarzi, M. (2018). Multi-attribute optimization of a novel micro liquid block working with green graphene nanofluid regarding preferences of decision maker. *Applied Thermal Engineering*, 143, 11-21. <https://doi.org/10.1016/j.applthermaleng.2018.07.074>
- Bazdidi-Tehrani, F., Khabazipur, A., Vasefi, S. I. (2018). Flow and heat transfer analysis of  $TiO_2$ /water nanofluid in a ribbed flat-plate solar collector. *Renewable energy*, 122, 406-418. <https://doi.org/10.1016/j.renene.2018.01.056>

- Bazdidi-Tehrani, F., Vasefi, S. I., Anvari, A. M. (2019). Analysis of particle dispersion and entropy generation in turbulent mixed convection of CuO-water nanofluid. *Heat Transfer Engineering*, 40(1-2), 81-94. <https://doi.org/10.1080/01457632.2017.1404828>
- Barzegarian, R., Moraveji, M. K., Aloueyan, A. (2016). Experimental investigation on heat transfer characteristics and pressure drop of BPHE (brazen plate heat exchanger) using TiO<sub>2</sub>-water nanofluid. *Experimental Thermal and Fluid Science*, 74, 11-18. <https://doi.org/10.1016/j.expthermflusci.2015.11.018>
- Choi, S. U., Eastman, J. A. (1995). Enhancing thermal conductivity of fluids with nanoparticles (No. ANL/MSD/CP-84938; CONF-951135-29). Argonne National Lab.(ANL), Argonne, IL (United States).
- Esfe, M. H., Yan, W. M., Akbari, M., Karimipour, A., Hassani, M. (2015). Experimental study on thermal conductivity of DWCNT-ZnO/water-EG nanofluids. *International Communications in Heat and Mass Transfer*, 68, 248-251. <https://doi.org/10.1016/j.icheatmasstransfer.2015.09.001>
- Hamad, M. A. A., Pop, I., Ismail, A. M. (2011). Magnetic field effects on free convection flow of a nanofluid past a vertical semi-infinite flat plate. *Nonlinear Analysis: Real World Applications*, 12(3), 1338-1346. <https://doi.org/10.1016/j.nonrwa.2010.09.014>
- Hemmat Esfe, M., Saedodin, S., Yan, W. M., Afrand, M., Sina, N. (2016). Study on thermal conductivity of water-based nanofluids with hybrid suspensions of CNTs/Al<sub>2</sub>O<sub>3</sub> nanoparticles. *Journal of Thermal Analysis and Calorimetry*, 124, 455-460. doi: 10.1007/s10973-015-5104-0
- Huang, D., Wu, Z., Sunden, B. (2015). Pressure drop and convective heat transfer of Al<sub>2</sub>O<sub>3</sub>/water and MWCNT/water nanofluids in a chevron plate heat exchanger. *International journal of heat and mass transfer*, 89, 620-626. <https://doi.org/10.1016/j.ijheatmasstransfer.2015.05.082>
- Ishak, A., Nazar, R., Pop, I. (2009). MHD convective flow adjacent to a vertical surface with prescribed wall heat flux. *International Communications in Heat and Mass Transfer*, 36(6), 554-557. <https://doi.org/10.1016/j.icheatmasstransfer.2009.02.012>
- Karimipour, A., Taghipour, A., Malvandi, A. (2016). Developing the laminar MHD forced convection flow of water/FMWNT carbon nanotubes in a microchannel imposed the uniform heat flux. *Journal of Magnetism and Magnetic Materials*, 419, 420-428. <https://doi.org/10.1016/j.jmmm.2016.06.063>
- Khairul, M. A., Alim, M. A., Mahbulul, I. M., et al. (2014). Heat transfer performance and exergy analyses of a corrugated plate heat exchanger using metal oxide nanofluids. *International Communications in Heat and Mass Transfer*, 50, 8-14. <https://doi.org/10.1016/j.icheatmasstransfer.2013.11.006>
- Miri, R., Abbassi, M. A., Ferhi, M., Djebali, R. (2022). Second law analysis of mhd forced convective nanoliquid flow through a two-dimensional channel. *acta mechanica et automatica*, 16(4), 417-431. doi: 10.2478/ama-2022-0050
- Miri, R., Mliki, B., Mohamad, B. A., Abbassi, M. A., Oreijah, M., Guedri, K., Abderafi, S. (2023). Entropy generation and heat transfer rate for MHD forced convection of nanoliquid in presence of viscous dissipation term. *CFD Letters*, 15(12), 77-106. <https://doi.org/10.37934/cfdl.15.12.77106>
- Miri, R., Mliki, B., Ayed, L., Abbassi, M. A., Djebali, R., Hidouri, A. (2024). Numerical Study of Magnetohydrodynamic Forced Convective Nanoliquid Flow Through a Channel with Backward Facing Step and Three Hot Cylinder Blocks. *Journal of Nanofluids*, 13 (4), 889-906(18). <https://doi.org/10.1166/jon.2024.2184>
- Mliki, B., Abbassi, M. A., Omri, A., Belkacem, Z. (2017). Lattice Boltzmann analysis of MHD natural convection of CuO-water nanofluid in inclined C-shaped enclosures under the effect of nanoparticles Brownian motion. *Powder Technology*, 308, 70-83. <https://doi.org/10.1016/j.powtec.2016.11.054>
- Nikelham, A., Enjilela, V., et al. (2022). The effects of magnetic-field direction and magnitude on forced convection of aluminum oxide-water nanofluid over a circular cylinder. *International Journal of Thermal Sciences*, 173, 107398. <https://doi.org/10.1016/j.ijthermalsci.2021.107398>
- Omiddezyani, S., Khazaei, I., Gharehkhani, S., Ashjaee, M., Shemirani, F., Zandian, V. (2019). Experimental

- Investigation of Convective Heat Transfer of Ferro-Nanofluid Containing Graphene in a Circular Tube under Magnetic Field. *Modares Mechanical Engineering*, 19(8), 1929-1941.
- Ravisankar, B., Chand, V. T. (2013). Influence of nanoparticle volume fraction, particle size and temperature on thermal conductivity and viscosity of nanofluids-A review. *International Journal of Automotive and Mechanical Engineering*, 8, 1316-1338. <https://doi.org/10.15282/ijame.8.2013.20.0108>
- Santra, A. K., Sen, S., Chakraborty, N. (2009). Study of heat transfer due to laminar flow of copper–water nanofluid through two isothermally heated parallel plates. *International journal of thermal sciences*, 48(2), 391-400. <https://doi.org/10.1016/j.ijthermalsci.2008.10.004>
- Selimefendigil, F., Öztop, H. F. (2018). Magnetic field effects on the forced convection of CuO-water nanofluid flow in a channel with circular cylinders and thermal predictions using ANFIS. *International Journal of Mechanical Sciences*, 146, 9-24. <https://doi.org/10.1016/j.ijmecsci.2018.07.011>
- Selimefendigil, F., Öztop, H. F., Chamkha, A. J. (2020). Role of magnetic field on forced convection of nanofluid in a branching channel. *International Journal of Numerical Methods for Heat & Fluid Flow*, 30(4), 1755-1772. doi: 10.1108/HFF-10-2018-0568
- Sheikholeslami, M., Vajravelu, K., Rashidi, M. M. (2016). Forced convection heat transfer in a semi annulus under the influence of a variable magnetic field. *International journal of heat and mass transfer*, 92, 339-348. <https://doi.org/10.1016/j.ijheatmasstransfer.2015.08.066>
- Sheikholeslami, M., Bhatti, M. M. (2017). Forced convection of nanofluid in presence of constant magnetic field considering shape effects of nanoparticles. *International Journal of Heat and Mass Transfer*, 111, 1039-1049. <https://doi.org/10.1016/j.ijheatmasstransfer.2017.04.070>
- Tassone, A., Nobili, M., Caruso, G. (2018). Numerical study of the MHD flow around a bounded heating cylinder: Heat transfer and pressure drops. *International Communications in Heat and Mass Transfer*, 91, 165-175. doi: 10.1016/j.icheatmasstransfer.2017.12.010
- Tumse, S., H. Zontul, H. Hamzah, B. Sahin, (2022), Numerical Investigation of magnetohydrodynamic forced convection and entropy production of ferrofluid around a confined cylinder using wire magnetic sources. *Arabian Journal for Science and Engineering*, 1-30. doi: 10.1007/s13369-022-07470-5
- Udhayakumar, S., AD, A. R., Sekhar, T. V. S., Sivakumar, R. (2016). Study of directional control of heat transfer and flow control in the magnetohydrodynamic flow in cylindrical geometry. *International Journal of Heat and Fluid Flow*, 61, 482-498. <https://doi.org/10.1016/j.ijheatfluidflow.2016.06.011>
- Vasefi, S. I., Bazdidi-Tehrani, F., Sedaghatnejad, M., Khabazipur, A. (2019). Optimization of turbulent convective heat transfer of CuO/water nanofluid in a square duct: An artificial neural network analysis. *Journal of Thermal Analysis and Calorimetry*, 138, 517-529. <http://dx.doi.org/10.1007/s10973-019-08128-5>

---

(2024) ; <http://www.jmaterenvironsci.com>